Nuclear Instruments and Methods in Physics Research A 659 (2011) 289–298

Contents lists available at SciVerse ScienceDirect

Nuclear Instruments and Methods in Physics Research A

journal homepage: www.elsevier.com/locate/nima

Vibrational excitation induced by electron beam and cosmic rays in normal and superconductive aluminum bars

M. Bassan [b,c], B. Buonomo [a], G. Cavallari [e,1], E. Coccia [b,c], S. D'Antonio [b], V. Fafone [b,c], L.G. Foggetta [a,2], C. Ligi [a,*], A. Marini [a], G. Mazzitelli [a], G. Modestino [a], G. Pizzella [c,a], L. Quintieri [a], F. Ronga [a], P. Valente [d], S.M. Vinko [a,3]

[a] Istituto Nazionale di Fisica Nucleare, Laboratori Nazionali di Frascati, Via E. Fermi, 40, 00044 Frascati, Italy
[b] Istituto Nazionale di Fisica Nucleare, Sezione Roma2, Via della Ricerca Scientifica, 00133 Rome, Italy
[c] Dipartimento di Fisica, Università di Tor Vergata, Via della Ricerca Scientifica, 00133 Rome, Italy
[d] Istituto Nazionale di Fisica Nucleare, Sezione Roma1, piazzale Aldo Moro 2, 00185 Rome, Italy
[e] CERN, CH1211, Genève, Switzerland

ARTICLE INFO

Article history:
Received 9 June 2011
Received in revised form
2 August 2011
Accepted 15 August 2011
Available online 22 August 2011

Keywords:
Gravitational wave detectors
Cosmic rays
Radiation acoustics

ABSTRACT

We report new measurements of the acoustic excitation of an Al5056 superconductive bar when hit by an electron beam, in a previously unexplored temperature range, down to 0.35 K. These data, analyzed together with previous results of a dedicated experiment obtained for $T > 0.54$ K, show a vibrational response enhanced by a factor ~ 4.9 with respect to that measured in the normal state. This enhancement explains the anomalous large signals due to cosmic rays previously detected in the NAUTILUS gravitational wave detector.

© 2011 Elsevier B.V. All rights reserved.

1. Introduction

Cosmic ray showers can excite sudden mechanical vibrations in a metallic cylinder at its resonance frequencies; in experiments searching for gravitational waves (*gw*) these disturbances are hardly distinguishable from the searched signal and represent an undesired source of accidental events, thus increasing the background. This effect was suggested many years ago and a first search was carried out with limited sensitivity with room temperature Weber type resonant bar detectors and ended with a null result [1]. Later on, the cryogenic resonant *gw* detector NAUTILUS [2] was equipped with a streamer tube extensive air shower detector [3] and the interaction of cosmic ray with the antenna has been studied in detail. This apparatus allowed the first detection of cosmic ray signals in a *gw* antenna, that took place in 1998, when NAUTILUS was operating at a temperature $T=0.14$ K [4], i.e. below the superconducting (s) transition of this aluminum alloy ($T_c \simeq 0.9$ K). During this run many events of very large amplitude were detected. This unexpected result prompted the construction, in 2002, of a scintillator cosmic ray detector also for the EXPLORER *gw* detector as well as the beginning of a dedicated experiment (RAP) [5], that was planned at the INFN Frascati National Laboratory to study the vibration amplitude of a small Al5056 bar caused by the hits of a 510 MeV electron beam. The experiment was also motivated by the need of a better definition of the thermophysical parameters of the alloy Al5056, used in the bar detector, at low temperatures. A detailed study of this effect is indeed useful to study the performance of *gw* bar detectors for exotic particles [6] and to understand the noise due to cosmic rays in interferometric *gw* detectors [7]. In this paper we summarize our previous knowledge on this effect. We then report the final results of the RAP experiments presenting measurements down to 0.35 K, and show how these new data help in shedding light on the 1998 anomalous NAUTILUS high energy events. We also recall that the detailed study of this thermo-acoustic effect has applications in devices used to monitor and measure particle beams characteristic, and in particular in monitoring high power beams [8].

2. The Thermo-Acoustic Model

2.1. The model: normal conductive (n) state

Beron and Hofstadter [9,10] first measured mechanical oscillations in piezoelectric disks hit by a high energy electron beam. The

* Corresponding author. Tel.: +39 0694032622; fax: +39 0694032256.
E-mail address: carlo.ligi@lnf.infn.it (C. Ligi).
[1] Honarary member of CERN.
[2] Now at Laboratoire de l'Accèlerateur Linaire, CNRS-Orsay, 91898 Orsay cedex, France.
[3] Now at Department of Physics, Clarendon Laboratory, University of Oxford, Parks Road, Oxford OX1 3PU, UK.

0168-9002/$ - see front matter © 2011 Elsevier B.V. All rights reserved.
doi:10.1016/j.nima.2011.08.028

authors first pointed out that cosmic ray events could excite mechanical vibrations in a *gw* resonant bar and that, consequently, cosmic rays could represent a background for experiments aimed at the detection of *gw*. The interaction of a ionizing particle with the bulk of a suspended cylindrical bar generates a pressure pulse in the bar. More in detail, the energy lost by the particle in the bar causes a local warming up of the material; the local thermal expansion in the bulk generates the pressure wave. This sonic pulse determines the excitation of the vibrational elastic modes of the suspended bar.

Grassi Strini et al. [11] reported the results of an experiment based on a pure aluminum bar exposed to a proton beam. The experimental data were compared to a theoretical model based on the Fourier response of a thin bar to the pressure wave originated by a delta-like thermal perturbation. If the heating is in the bar center, only even Fourier harmonics are allowed. The "maximum amplitude of oscillation for the fundamental longitudinal elastic mode", in the following referred to as "Amplitude", for a material in a normal (n) state of conducting is given, according to this Thermo-Acoustic Model (TAM), by

$$B_n^{th} = \frac{2\alpha LW}{\pi c_V M} \tag{1}$$

where the suffix "*th*" stand for the theoretically expected value. This result applies to a thin cylinder (with radius R and length L, $R \ll L$ and mass M), for a beam hitting on center of the cylinder lateral surface. Here W is the total energy released by the beam to the bar, α is the linear thermal expansion coefficient and c_V is the isochoric specific heat. The dimensionless Grüneisen parameter γ of the material includes the α/c_V ratio:

$$\gamma = \frac{\beta K_T}{\rho c_V} \tag{2}$$

where β is the volume thermal expansion coefficient ($\beta = 3\alpha$ for cubic elements), K_T is the isothermal bulk elastic modulus and ρ is the material density. The Grüneisen γ slightly depends on the temperature when the material is in the n state.

Eq. (1) is a limit case of a more general problem, when the paths of the interacting particles in the bulk [12–14] are considered. Introducing a vector field $\mathbf{u}(\mathbf{x},t)$ describing the local displacements from equilibrium, the amplitude of the k-th mode of the cylinder oscillation is proportional to

$$g_k^{therm} = \frac{\Delta P^{therm}}{\rho}\mathcal{A}'\mathcal{I}_k = \frac{\gamma}{\rho}\left|\frac{dW}{dx}\right|\mathcal{I}_k \tag{3}$$

where ΔP^{therm} is the pressure pulse due to the sonic source described above, dW/dx is the specific energy loss of the interacting particle, $\mathcal{A}'$ is the cross-section of the tubular zone centered on the particle path in which the effects are generated and $\mathcal{I}_k = \int dl(\nabla \cdot \mathbf{u}_k(\mathbf{x}))$ is a line integral over the particle path involving the normal mode of oscillation $\mathbf{u}_k(\mathbf{x})$. The Amplitude predicted by Eq. (1), can be rederived from Eq. (3) in the simplified case of a thin bar ($R/L \ll 1$) and for a particle hitting on the bar center. We can therefore adjust the value of Amplitude predicted by Eq. (1) to a more correct value:

$$B_n^{th} = \frac{2\alpha LW}{\pi c_V M}(1+\varepsilon) \tag{4}$$

where ε is a corrective parameter estimated by a Monte Carlo (MC) simulation [5], which takes into account the solutions $O[(R/L)^2]$ for the modes of oscillation of a cylinder, the transverse dimension of the beam at the impact point and the trajectories of the secondary particles generated in the bar. The value of ε for the bar used in the experiment is estimated by MC to be -0.04.

2.2. The model: superconducting (s) state

When the material is in the s state, a part of the energy lost by particle causes the suppression of the superconductivity in a region, called hot spot, that is centered around the particle path. The maximum possible radius of the hot spot, r_{HS}, is obtained by equating the specific energy lost by the particle, dW/dx, to the enthalpy variation (per unit volume), Δh, for the transition from the s state at temperature T to the n state [15–18]:

$$r_{HS} = \sqrt{\frac{\mathcal{A}''}{\pi}} = \sqrt{\frac{|dW/dx|}{\pi \Delta h}} \tag{5}$$

where $\mathcal{A}''$ is the cross-section of the zone switched to the n state.

The creation of a hot spot by a particle interacting with a material in s state causes a further correction to Amplitude of Eq. (4), a term which is peculiar to the particle propagating in a zone now switched to the n state. The additional contribution to the amplitude of the cylinder oscillation mode k is proportional to [12,13]

$$g_k^{trans} = \frac{\Delta P^{trans}}{\rho}\mathcal{A}''\mathcal{I}_k = \frac{1}{\rho}\left[K_T\frac{\Delta V}{V} + \gamma T\frac{\Delta \mathcal{S}}{V}\right]\mathcal{A}''\mathcal{I}_k.$$

Here ΔV and $\Delta \mathcal{S}$ are the differences of the volume and entropy in the two states of conduction. The differences can be expressed in terms of the thermodynamic critical field H_c and it follows [19], in first approximation, that[4]:

$$\frac{\Delta V}{V} = \frac{V_n - V_s}{V} = \frac{H_c}{4\pi}\frac{\partial H_c}{\partial P}$$

and

$$\frac{\Delta \mathcal{S}}{V} = \frac{\mathcal{S}_n - \mathcal{S}_s}{V} = -\frac{H_c}{4\pi}\frac{\partial H_c}{\partial T}.$$

The quadratic dependence $H_c(t) = H_c(0)(1-t^2)$ on t, where $t = T/T_c$, is assumed in computing the differences.

Therefore, the value of Amplitude due to a particle creating hot spots in a material in s state is given by

$$B_s^{th} = B_n^{th}(1+\mathcal{R}) = B_n^{th}\left[1 + \left(\Pi\frac{\Delta V}{V} + T\frac{\Delta \mathcal{S}}{V}\right)(\Delta h)^{-1}\right] \tag{6}$$

where $\mathcal{R} = g_k^{trans}/g_k^{therm}$ and the definition (2) of γ is used to obtain

$$\Pi = \frac{2\rho L(1+\varepsilon)}{3\pi M\frac{B_n^{th}}{W}}.$$

Eqs. (4) and (6) show, by inspection, that the Amplitude B^{th} linearly depends on W, the energy released by particle, both in the n and s states. Therefore, it appears natural to consider, as we do in the following, the ratio B^{th}/W as a measure of the relevant material properties. Finally we note that the knowledge of the specific heat of the material for the s state, c_s, allows us to approximate the exact Eq. (5) with the following condition for the transition s→n of a volume V of the material at temperature T, due to the absorption of energy W from the particle [15,17]:

$$W > VC_I(T) \tag{7}$$

[4] We keep the CGS electro-magnetic system of units for the magnetic field, as used by the authors of the cited articles, and we convert the density of the magnetic energy to SI units.

with

$$C_I(T) = \int_T^{T_c} c_s(T')\, dT'.$$

Moreover, the knowledge of $c_s(T)$ allows to derive Δh from the relation $\Delta h(T) = C_I(T) + T\Delta\mathcal{S}/V$ [20].

2.3. Amplitude predictions for the normal and superconductive state

In order to compute, by means of Eq. (4), the expected value of Amplitude at different temperatures, we need, for the n state, both $\alpha(T)$ and $c_V(T)$ of the material. As these values are not well known for the Al5056 alloy, we used those of pure aluminum. Polynomial interpolations on data of Ref. [21] ($12 < T \leq 300$ K) and the parametrization in Ref. [22] ($T \leq 12$ K) give $\alpha(T)$, while $c_V(T)$ is obtained by polynomial interpolations on values of c_P reported in Ref. [23]. Table 1 shows the computed values of α, c_V and the normalized Amplitude B_n^{th}/W.

For the s state instead, measurements performed at very low temperatures [24] on samples belonging to the same production batch of our Al5056 bars, allow us to characterize the relevant properties of that alloy. The measurement of the transition temperature to the s state, carried out using the mutual inductance method, yields $T_c = 0.845 \pm 0.002$ K and a total transition width of about 0.1 K. Few data of specific heat for Al5056 are available in the literature [25]; however, new c_V measurements were performed above and below T_c [24].

In the temperature interval $0.9 \leq T \leq 1.5$ K, i.e. in the n state, assuming for the specific heat the usual low temperature parametrization: $c_V = \Gamma T + \Psi T^3$, the measurements give the values $\Gamma = 1157 \pm 31$ erg cm^{-3} K^{-2} for the electronic specific heat coefficient and $\Psi = 140 \pm 10$ erg cm^{-3} K^{-4} for the lattice contribution.

On the other hand, computing the Amplitude in the s state by means of Eq. (6) requires the knowledge of (a) the thermophysical parameters α_n and $c_{V,n}$ of the material, in order to evaluate B_n for the n state below T_c and (b) the dependence of H_c on T and P for calculating the derivatives $\partial H_c/\partial T$ and $\partial H_c/\partial P$. The requirement (a) cannot be fulfilled due to the lack of knowledge of α_n for Al5056 and we therefore assume for B_n/W the value measured just above T_c. This assumption is justified by the fact that γ_n usually has, below T_c, a very weak dependence on temperature. Regarding requirement (b), we derive $\partial H_c/\partial T$ at $T < T_c$ from the H_c parabolic dependence on t; we also assume that the unknown dependence of $\partial H_c/\partial P$ on t at $P=0$ for Al5056 is equal to that of pure aluminum and, therefore, can be obtained from the tabulation of H_c as a function of T and P contained in Ref. [26]. If the superconducting properties of Al5056 can be described by the BCS theory, then $H_c(0) \approx 2.42\Gamma^{1/2}\ T_c \approx 70$ Oe. Insertion of the numerical values in the Eq. (6) yields to values of B_s/W ranging from -9.2×10^{-10} to -7.3×10^{-10} mJ^{-1} in the temperature interval having limits 0.3 and 0.8 K, respectively. The lower limit of the temperature interval is constrained by the data availability in the $H_c(P,T)$ tabulation of Ref. [26].

Table 1
Normal state of conduction. Amplitude normalized to the beam released energy W and input values for the calculation (α,c_V) in the case of the RAP bar ($L=0.5$ m; $M=34.1$ kg) made of pure aluminum. The correction of Eq. (4) is applied.

T (K)	α (10^{-6} K^{-1})	c_V (J mol^{-1} K^{-1})	B_n^{th}/W (10^{-10} mJ^{-1})
264	22.2	23.5	2.23
71	7.5	7.94	2.23
4.5	5.8×10^{-3}	7.6×10^{-3}	1.80
1.5	1.5×10^{-3}	2.1×10^{-3} [a]	1.72

[a] c_V value for Al5056.

3. The RAP experimental setup

3.1. The bar and the piezoelectric ceramics

The RAP experiment has been fully described in Ref. [5]. Here we briefly recall that the test mass is a cylindrical bar ($R=0.091$ m, $L=0.5$ m, $M=34.1$ kg) made of Al5056, the same aluminum alloy (nominal composition 5.2% Mg and 0.1% of both Cr and Mn) used for NAUTILUS. The bar hangs from the cryostat top by means of a multi-stage suspension system ensuring attenuation from the external mechanical noise of -150 dB in the 1700–6500 Hz frequency window. The frequency of the fundamental longitudinal mode of oscillation of the bar is $f_0 = 5414.31$ Hz below $T=4$ K.

At temperatures below 10 K, the Al5056 intrinsic Q factor is 4.1×10^7 [27] corresponding to a decay time of the order of 20 min: a shorter decay time is desirable in order to have a more manageable repetition rate of the hits. This is simply achieved by the presence of a thermometer on one of the bar faces, that damps the oscillations to a decay time of the order of 30 s. Therefore, we only have to wait a couple of minutes between consecutive hits to avoid the pile-up of the signals.

Two piezoelectric ceramics (Pz), electrically connected in parallel, are inserted in a slot milled out in the center section of the bar, opposite to the bar suspension point, and are squeezed when the bar shrinks. In this Pz arrangement the strain measured at the bar center is proportional to the displacement of the bar end faces. The Pz output is first amplified, and then sampled at 100 kHz by an ADC embedded in a VME system, hosting the data acquisition system. A band pass filter between 300 Hz and 50 kHz is used to reduce the low frequency power line noise and to avoid Fourier aliasing.

The measurement of the Pz conversion factor λ, relating voltage to oscillation amplitude, is accomplished according to a procedure [28] based on the injection in the Pz of a sinusoidal waveform of known amplitude, with frequency f_0 and time duration less than the decay time of the mechanical excitations and on the subsequent measurement of Amplitude. The procedure is correct if $R/L \ll 1$ and carries a 6% systematic error.

The value of λ during the 2009 run was 1.26×10^7 V m^{-1} at room temperature and 1.16×10^7 V m^{-1} constant at temperature $T \leq 4.5$ K.

3.2. The Frascati DAΦNE beam test facility

The DAΦNE BTF transfer line can transport and deliver in controlled way electron or positron beams, from the end of the Linac to a 100 m^2 experimental hall, where users normally carry out their tests and experiments. A more detailed description of the layout of the BTF transfer line and of the RAP experimental set-up can be found in Ref. [5]. Particles can be provided in 1 or 10 ns duration pulses, with an injection frequency spanning from 1 to 50 Hz,[5] in a wide energy range (25–750 MeV for electrons) and intensity (from 1 up to 10^{10} particles/pulse). Since the end of 2004, when the RAP experiment was first operated with the aluminum bar, some important upgrades [29] and diagnostic improvements [30] have been accomplished. The most important improvement concerned the installation, during the 2006 shutdown, of a pulsed dipole magnet at the end of the Linac: such magnet allows to alternate the beam between the DAΦNE damping rings and the test beam area, thus enhancing the BTF duty cycle, due to the reduced switching time.

[5] Actually one of the 50 pulses in 1 s is sent to an hodoscope in order to reconstruct the energy profile of the beam at the end of the Linac.

The beam multiplicity for the RAP measurements performed in 2009 spanned from 10^7 to 10^9 electrons per bunch of 10 ns time-length. The current intensity modulation was obtained by properly changing the aperture of the tungsten slits (both horizontal and vertical ones) along the BTF transfer line: this procedure, unlike that used in the previous RAP measurement campaign, based on the defocusing of the beam by quadrupoles, allows to avoid the beam degradation, since the particles in the external tails are cut away.

For the beam diagnostics, a monitor (WCM), based on an integrating current transformer, readout by a charge digitizer, was used to measure the pulse charge. The device accuracy is 3% and the readout noise fluctuations give a measurement error $\sigma = 1.5 \times 10^7$ electrons. The device is equipped with a calibration coil used to control the gain, the noise and the time shaping of the generated signals.

3.3. Cryogenic setup

The RAP cryogenic setup consists of a KADEL commercial liquid helium cryostat, 3.2 m high and 1 m in diameter, suspended on a vertically movable structure, and containing a dilution refrigerator. A schematic view of the cryostat together with the cold side of the dilution refrigerator is depicted in Fig. 1.

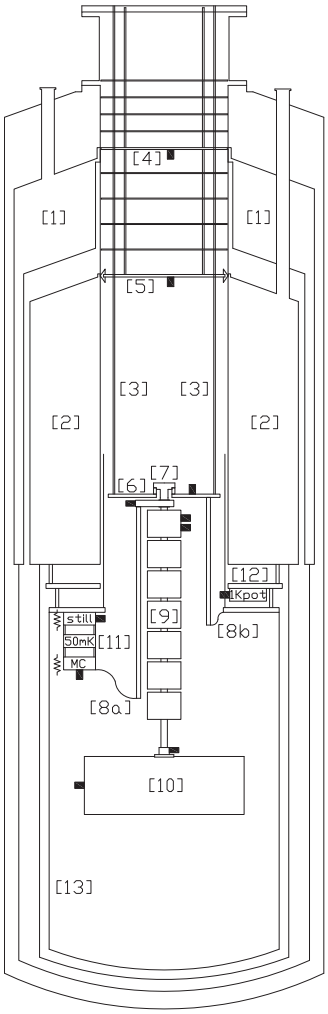

Fig. 1. Schematic view of the RAP cryostat: [1] LN_2 reservoir, [2] LHe container, [3] Stainless Steel (SS) suspension cables, [4] 77 K flange, [5] 4.2 K flange, [6] 0.6 K flange, [7] SS screw with Teflon ring, [8a and 8b] thermal contacts, [9] copper suspension, [10] bar, [11] dilution refrigerator cold end, [12] 1 K Pot, and [13] radiation shields. The filled squares represent the thermometers.

The liquid helium (LHe) and liquid nitrogen (LN_2) dewars, with a capacity of 340 L and 200 L, respectively, are placed in the upper half. Three stainless steel cables are suspended from the top flange to support the experimental apparatus. To avoid the radiation input, eight aluminum radiation shields are mounted between the top flange at room temperature, the 77 K OFHC (Oxygen Free, High Conductivity) copper flange and the 4.2 K OFHC copper flange. These two latter flanges are mechanically connected with the LN_2 and LHe dewars, respectively. The experimental chamber is positioned on the lower half of the cryostat and is surrounded by one OFHC copper radiation shield connected to the Still flange, two aluminum radiation shields connected to the LHe dewar and the LN_2 dewar, respectively, and the outer aluminum container. The LHe container is indium sealed to separate the experimental chamber volume from the insulation zone.

The cryostat hosts a continuous flow, closed cycle ^{3}He–^{4}He dilution refrigerator, made by Leiden Cryogenics, with a base temperature of about 100 mK and a cooling power of about 1 mW at 120 mK. The continuous flow is ensured by a pumping system, composed of two Varian TV 551 NAV turbo-molecular pumps and an Edwards XDS 35 scroll pump. A Gas Handling System control panel manages the mixture flow in the circuit lines, either automatically or manually. In automatic operation a CPU running a software program, that reads measures from several Pirani pressure gauges and a flow meter placed in the circuit line, manages the flow operating a number of solenoid valves. Temperatures of the experimental setup are measured by 11 thermometers of three different types (Pt1000, FeRh and RuO_2 resistances), connected to an AVS-45 and an AVS-47 Picowatt Resistance Bridges. The resolution of the RuO_2 thermometers at the lowest temperatures is 0.25 mK. The cryostat is also equipped by four vacuum gauges and a LHe level gauge. Inside the dilution refrigerator there are two capacitance gauges that measure the liquid level in the 1 K Pot (a pumped LHe bath in thermal contact with the fridge line where the incoming ^{3}He–^{4}He mixture condenses), and in the Still. All diagnostic data are gathered, via serial and GPIB interfaces, by a PC running a LabView program which displays the readings on a synoptic window and records all the measurements.

To avoid transmission of mechanical vibrations to the bar, the thermal links between the cold spots of the refrigerator and the experiment are kept to a minimum: (i) a couple of thin ($160 \times 50 \times 0.2$ mm) OFHC copper sheets between the Mixing Chamber and the top of the suspension (n. 8a in Fig. 1), and (ii) three thin sheets ($100 \times 16 \times 0.2$ mm), between the Still flange and the 0.6 K flange (n. 8b in Fig. 1). These contacts assure the bar and suspension cooling when the dilution refrigerator is in operation, i.e. below 4 K. Above this temperature gas conduction provides the heat removal by inserting a few mbar of gaseous helium in the experimental chamber. The gas is then removed before reaching the liquefaction (about 5 K).

Cooling the cryostat to 80 K and filling the LN_2 dewar takes about 3 days and about 1000 L of LN_2. Twelve hours and about 800 L of LHe are sufficient to cool the system from 80 to 4.2 K and leave about 150 L of liquid in the dewar. The cryostat consumption, once thermalized, is about 1 L/h of LN_2 and about 1.5 L/h of LHe, that raises to about 2 L/h when the 1 K Pot is in operation.

The minimum temperature reached by the bar during the data taking was 343 mK, read by a RuO_2 thermometer placed at the center of one of the bar end faces.

3.4. RAP data collection and analysis

The piezoelectric signals were recorded by an ADC sampled at 100 kHz running under LabView control. At low temperature, due

to the low specific heat, the thermometer has sufficient sensitivity to measure the increase of the bar temperature after each shot. This additional information helped in monitoring the beam intensity. It was important to read this raise immediately after the hit, as the temperature rapidly relaxes back to its equilibrium value. For this reason, after the cooldown and during the beam measurement, we gave up multiplexing the thermometers, so that the thermometer on the bar end face can be read out with a rate of 1 Hz.

Fig. 2 shows the bar temperature measured during a low temperature run: it can be clearly seen that the bar is warmed up by the beam, and after each hit it relaxes to a higher temperature. To deal with this problem, the measurements were started at base temperature (343 mK) and taken with successively increasing temperature.

The 100 kHz ADC data were processed both online for a fast response and offline with a more sophisticated procedure. Figs. 3 and 4 show several important features of the signal. Fig. 3 shows the ADC output for a typical shot at low temperature; in the lower part of the figure the data are zoomed around the hit time in order to exhibit the sign of the first swing above the background (negative in the shown example); Fig. 4 shows the output in volt of the filtering procedure that selects the signal at the first longitudinal resonance. The filtered output is shown *vs* time from the start of the run.

Fig. 5 shows the Fourier power spectrum for the average of seven signals like the one in Fig. 3, after subtracting the noise spectra. The first two lines are the first flexural mode and the first longitudinal mode. We have studied in detail only the first longitudinal mode, because it is the one of interest for *gw* detectors. However, a quick analysis of the other modes did not show any relevant difference regarding the temperature dependence.

The Fourier component at the desired frequency f_0 (angular frequency ω_0) is extracted with a filtering algorithm known as "digital lock-in". For a hit at time t_0, corresponding to sample i_0, we create the time series:

$$c_{bkg} = \sum_{i=i_0-N}^{i_0-1} V_i \cos\left(\omega_0 \frac{i}{f_c}\right)$$

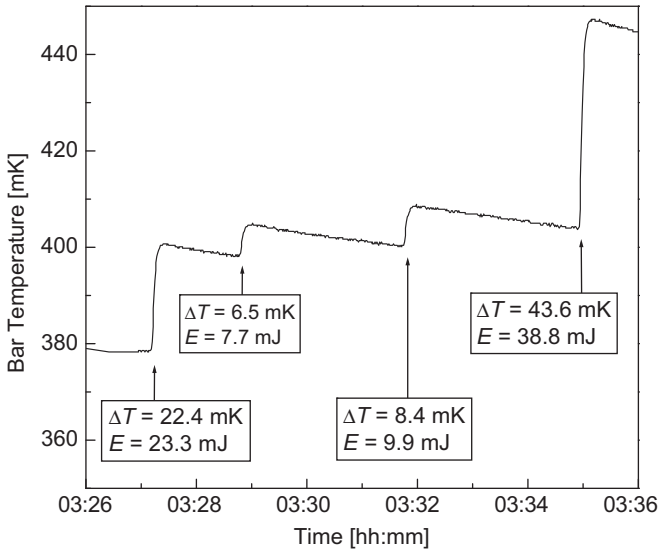

Fig. 2. Bar temperature measured during a run. Four beam shots are visible. The steps in temperature are proportional to the energy deposited in the bar. They can be used to measure the Al5056 specific heat, yielding a result in agreement with the measurement in Ref. [24]. Moreover, this information is useful to monitor the beam and to check the intensity measured by the current monitor.

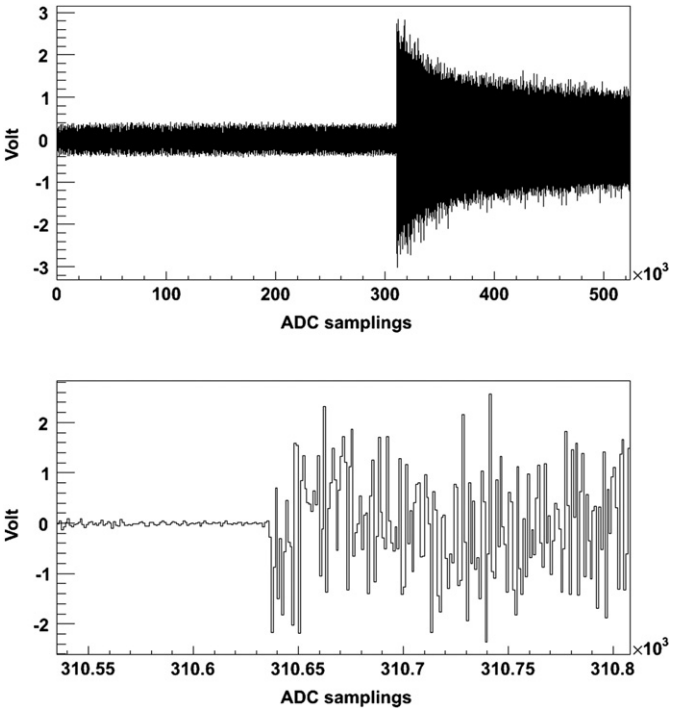

Fig. 3. Above: an example of a shot at $T=0.368$ K. After the shot the temperature raised to 0.405 K. The deposited energy was 30 mJ. The horizontal units are samples, the sampling time being 10 μs. Below: the zoom of the ADC output to show the sign of the first value above the background, in this case negative.

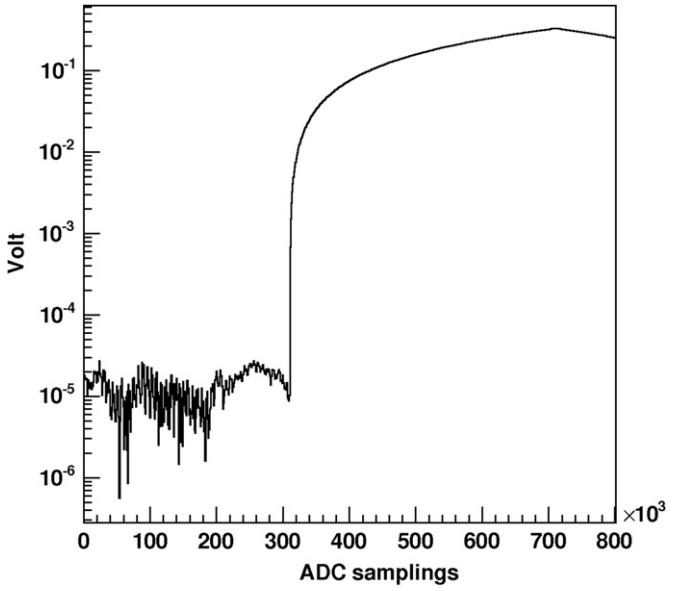

Fig. 4. The output of the filtering procedure that selects the signal component at the first longitudinal resonance *vs* time from the start of the run. The shot is the same of Fig. 3. The filtering procedure is most useful for small signals, when the amplitude is comparable to the noise.

$$c_{signal} = \sum_{i=i_0}^{i_0+N} V_i \cos\left(\omega_0 \frac{i}{f_c}\right)$$

where V_i is the i-th value of ADC output, f_c the sampling frequency and the number of samples considered is optimized with $N=400{,}000$. Similar quantities are computed for the quadrature (sine) component, and from the two we construct the complex amplitude before (noise) and after (signal) the hit. Taking the difference of these two amplitudes produces the desired filtered

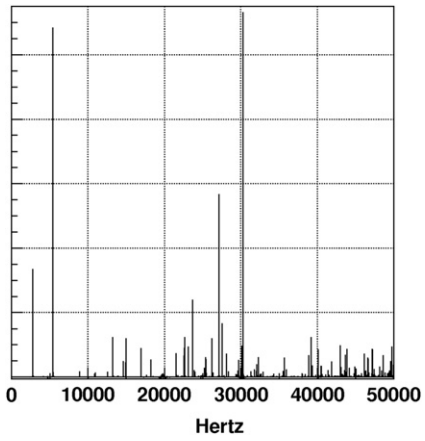

Fig. 5. The Fourier power spectrum for the average of seven signals like that shown in Fig. 3, after subtracting the noise spectrum. The first two spectral lines are the first flexural mode and the first longitudinal mode. The *y*-scale is in arbitrary unit.

output. A correction is applied to take into account the decay of the signal as function of the time.

4. The RAP measurement in superconducting state

We present in this section data of the last run of RAP at the Frascati BTF, that took place between June 30th and July 2nd 2009, just after the commissioning of the dilution refrigerator. We took data in the temperature range 0.344–257 K for a total of 164 beam shots on the bar and the energy deposited by each shot was in the range $1 \lesssim W \lesssim 70$ mJ. The data at high temperatures were in agreement with those of previous run and will not be discussed in this section. The 2007 measurements [31], performed at $T \geq 0.54$ K, are analyzed in this section together with the 2009 data. Some improvements introduced in this run, like the "lock-in filter", reduced the noise and increased the sensitivity at small energies.

The data taken at temperatures in the range $0.9 \leq T \leq 2$ K (i.e. above T_c), reported in Fig. 6, show a linear correlation between B, the maximum amplitude of the first longitudinal mode, and the released energy W, in agreement with the model of Section 2. The data of 2009 appear to be of better quality than those of 2007, due to the improvements in the beam stability and in the analysis procedure. The error bars are due to the combination of different sources:

- the noise in the measurement of the vibration amplitude: $\pm 1.3 \times 10^{-13}$ m,
- the uncertainty on the deposited energy (due to a reading error of the beam current): ± 0.8 mJ,
- the error in the temperature measurement, that also takes into account the local increase in the bar temperature after every shot and a possible nonuniform profile of the temperature along the bar: ± 0.01 K and
- an overall systematic error of the order of $\pm 6\%$, that accounts for the slightly different set-up and analysis procedures adopted in the 2007 and 2009 runs.

Both sets of data for temperature $T \leq 1.6$ K of the years 2007 and 2009 are shown in Fig. 7. This plot shows the measured B/W (with sign) as function of the temperature and of the deposited energy W. The most relevant features of this plot are:

- a constant value of B/W for $T \geq T_c$,
- a change of sign of B/W for $T \leq T_c$ and

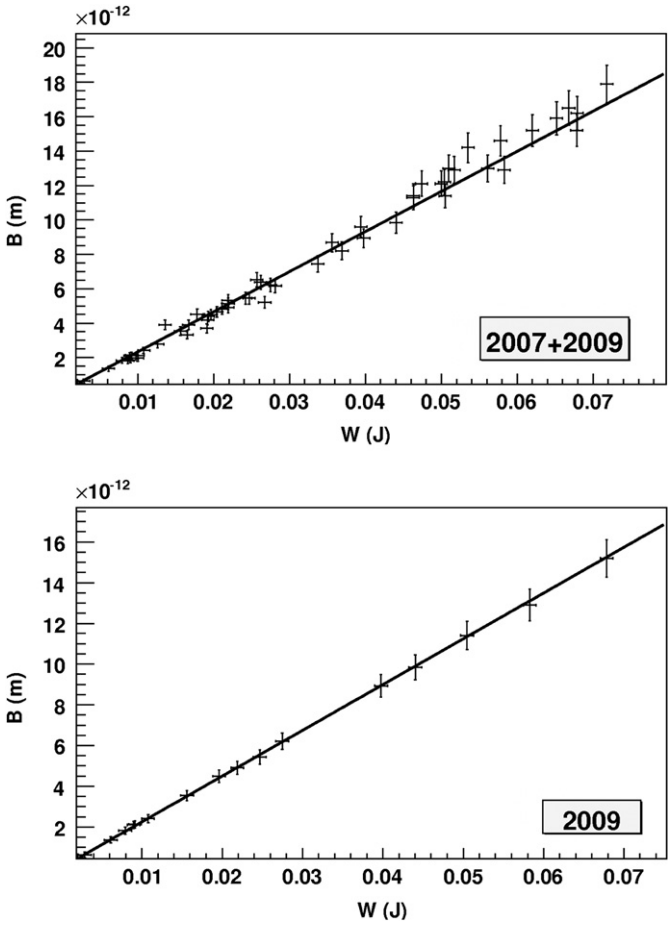

Fig. 6. The measured Amplitude of the first longitudinal mode B^{exp} *vs* the energy W deposited in the bar in the n state with $0.9 \leq T \leq 2$ K. The solid line is a linear fit constrained to the origin. The top figure represents all data from the 2007 and 2009 runs, while the bottom one shows only the 2009 data. The result of the fits are: $p_0 = (2.33 \pm 0.02) \times 10^{-10}$ m/J, $\chi^2/\text{ndf} = 51.69/55$(2007+2009 plot) $p_0 = (2.24 \pm 0.05) \times 10^{-10}$ m/J, $\chi^2/\text{ndf} = 0.4554/15$(2009 plot). The 2009 data have a better χ^2 due to the improvements in the beam stability and in the data analysis.

- a nonlinear dependence of B on W for $T \leq T_c$, not predicted by the model (Eq. (6)).

A change of sign for superconductive aluminum is to be expected, because the effect due to the s→n transition can lead to a negative sign due to the competitive terms in Eq. (6). We recall that the sign of B is inferred by the sign of the first value of the ADC over the noise after the beam shot (see Fig. 3b). The sign is positive for an expansion, negative for a contraction. The plot includes the measurement of NAUTILUS with cosmic rays described in Section 5. This value has been obtained from the ratio of the NAUTILUS data at $T=0.14$ K and the NAUTILUS data at $T=2$ K. The NAUTILUS point correspond to a value of the energy $W \sim 0.5$ μJ.

Fig. 8 shows the projection of these data in four intervals of deposited energy W. This figure helps to understand the data behavior, but is important to note that some time data do not overlap well, due to the strong dependence on W.

Fig. 8 shows that the data at the lowest deposited energies have a simple behavior: a plateau at very low temperatures, a plateau at higher temperature (above T_c) and a transition region in between. The first plateau disappears in the plots for higher energies.

As our investigation is aimed at understanding the interactions of cosmic rays with a *gw* detector, we need a model to make

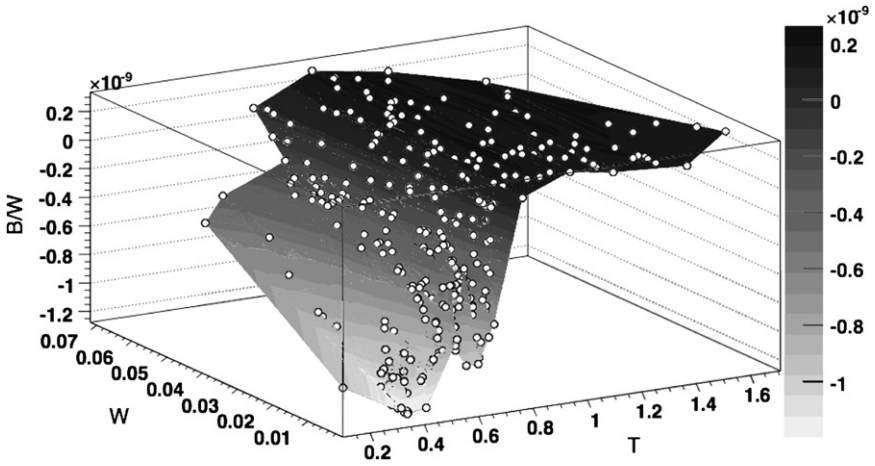

Fig. 7. Synoptic view of the data for temperature $T \leq 1.6$ K, the transition temperature is about 0.9 K. The plot shows the measured B/W [m/J] (with sign) *vs* temperature T [K] and deposited energy W [J]. The most relevant feature of this plot are: a constant value of B/W for $T \geq T_c$, the change of sign of B/W for $T \leq T_c$ and the dependence on W of B/W for $T \leq T_c$. The experimental data are the open circles. The shadowed regions are interpolations of the data. The point at the lowest temperature $T=0.14$ K is obtained from the cosmic ray NAUTILUS data.

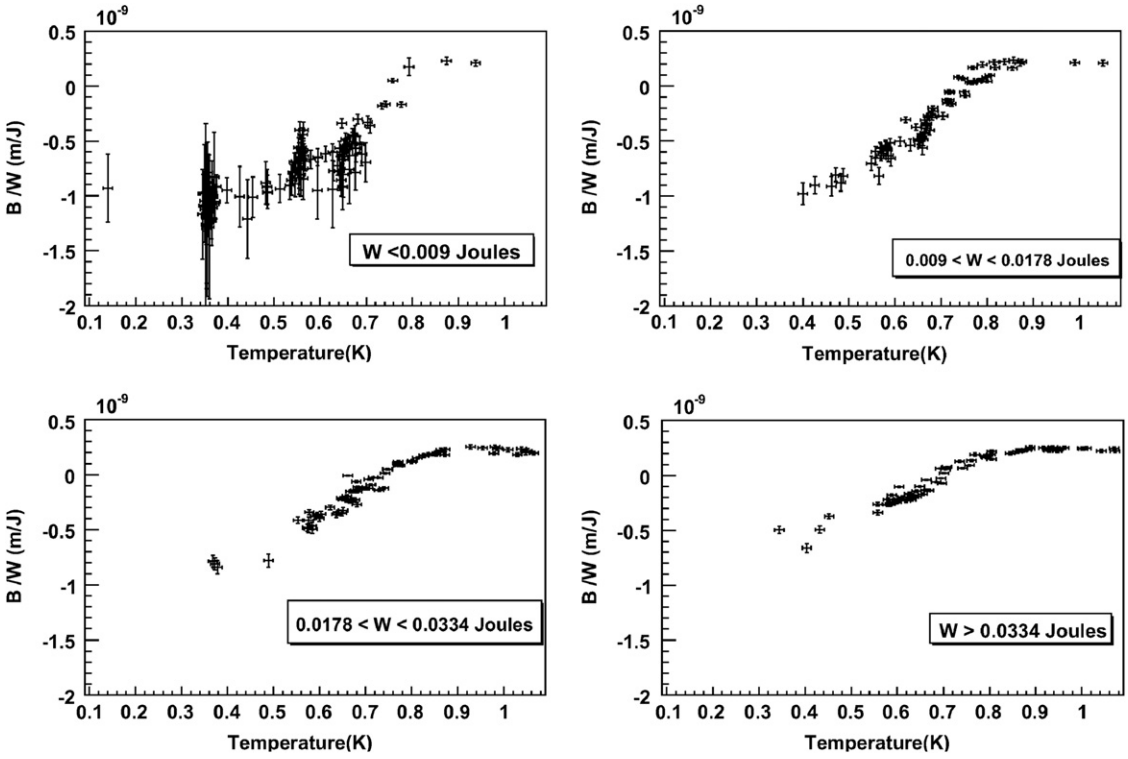

Fig. 8. Summary of the data for temperature $T \leq 1.1$ K. The plots show the projections of the data of Fig. 7 in 4 energy interval. Note that, due to the strong dependence on W, data points sometimes do not overlap well.

prediction of B/W at very small value of W: we have used the model described in Section 2, adding to it, as suggested by the data, a possible saturation of the s→n transition effect, due the high energy density in the volume crossed by the beam.

We can estimate this saturation effect starting from the radius of the cylindrical volume that switches from the s to n state around a particle leaving 195 MeV in the RAP aluminum bar (195 MeV is the mean value of the energy loss per each 510 MeV electron of the BTF beam). This critical radius R_c depends from the energy necessary to activate the transition. This energy can be computed in several ways [15], yielding consistent results. Using Eqs. (5) and (7) we have

$$R_c(T) = \sqrt{\frac{W}{\pi \rho l C_l(T)}} \tag{8}$$

where $l \sim 2R$ is the length of the path of the electron inside the bar.

Therefore, using the value of specific heat of Al5056 previously discussed and reported in Ref. [24], we obtain $R_c \sim 1\,\mu$m if $T=0.5$ K. The total cross surface interested by this transition for $N=10^9$ electrons is of the order $N\pi R_c^2 \sim 30$ cm^2, comparable to the

beam cross-section of the BTF beam, typically $\sim 20\,cm^2$. This is a crude estimate, but it shows that this effect can produce a nonlinear (with respect to the deposited energy W) response in the RAP data.

In order to extrapolate the RAP results to values of W and T outside the measured range, we used the following four parameters fit to the data for $T < T_c$:

$$\frac{B}{W} = a + (b(T) - a)\exp\left(\frac{-W}{p_0 \rho C_I(T)}\right) \quad (9)$$

$$b(T) = p_1 + p_2 T + p_3 T^2. \quad (10)$$

Here $a \sim 2.25 \times 10^{-10}\,mJ^{-1}$ is the constant value of B/W for $T > T_c$ obtained from Fig. 6 and $b(T)$ the value of B/W for $T < T_c$ and $W \to 0$. $b(T) \sim -10^{-9}\,mJ^{-1}$ for $T = 0.5$ K is a function weakly dependent on T and accounts for small variations of physical parameters at low temperatures. C_I is the integrated specific heat between T and the critical temperature, as defined in Eq. (7) and computed from the numerical values of Ref. [24]. Eq. (9) derives from the consideration that if an electron crosses a region that has already undergone the s→n transition, the response is the one of the n state.[6] The parameter p_0 is the bar volume intercepted by the electron beam.

In the measurement on a niobium bar [32] the complex pattern of Fig. 7, with the nonlinear behavior in W, was not observed. This is consistent with our model if we consider that niobium has a higher T_c and specific heat is much larger: C_I of niobium is indeed about two order of magnitude larger than C_I of aluminum for comparable value of the integration interval $T_c - T$. Therefore, the beam intensity in the niobium measurement was not enough to see saturation effects.

The result of the fit of Eq. (9) with these four parameters are given in Table 2. The data fit gives a $\chi^2/d.o.f. = 368/286 = 1.29$, slightly larger than one; this suggests that there are effects not taken into account.

Indeed, this simplified transition model cannot include all the effects: for example, the beam profile, the shower development inside the bar, the uncertainty of the critical temperature, possible unhomogeneity of the material, etc. are not accounted for. It is, however, remarkable that a very simple expression can describe the complicated pattern of Fig. 7.

Fig. 9 shows the fit residuals (measured data minus the fit predictions) *vs* temperature. The energy dependence seems to be well reproduced with the exception of the region just below T_c where there are more scattered points.

Table 3 summarizes the RAP results of B/W for Al5056 obtained with the RAP data from room temperature down to 0.14 K. The value and the errors for $T < T_c$ are obtained from the fit of Eq. (9) for $W \to 0$. The last value was obtained by extrapolating also with respect to the temperature down to $T = 0.14$ K, a temperature relevant for the comparison with NAUTILUS data that was, unfortunately, beyond the reach of our refrigerator. We note that the model described in Section 2 is quite accurate only for $T > T_c$. For $T < T_c$ there are the discrepancies that could be due either to a failure of the model or to uncertainties in the Al5056 superconductive parameters.

[6] Consider a beam bunch of high intensity, lasting a few nanoseconds (a time much shorter than the relaxation time needed to restore the s state) and involving a volume V_0 of the bar: the electrons that follow will probe a variable fraction of the volume V_0 switched from the s to the n state. The volume dV that undergoes the s→n transition for a deposited energy dW is

$$dV \sim \left(1 - \frac{V}{V_0}\right)\frac{dW}{\rho C_I} \quad (11)$$

Table 2
Parameters for the fit of Eq. (9) to the RAP data.

Parameter	value
$p_0\,(m^3)$	$(1.88 \pm 0.06) \times 10^{-3}$
$p_1\,(mJ^{-1})$	$(0.99 \pm 0.13) \times 10^{-9}$
$p_2\,(mJ^{-1}\,K^{-1})$	$(-1.31 \pm 0.43) \times 10^{-9}$
$p_3\,(mJ^{-1}\,K^{-2})$	$(-3.0 \pm 0.37) \times 10^{-9}$

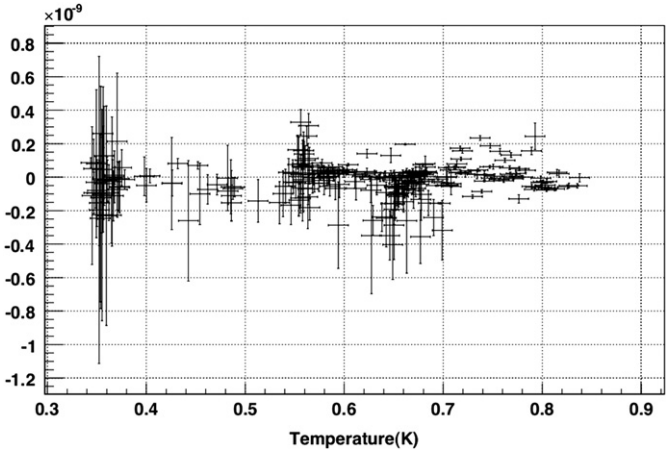

Fig. 9. Residuals of the fit of Eq. (9) to the RAP data *vs* temperature, overlapping on all energies.

Table 3
Summary of the values of B/W derived from measurements on Al5056. For $T > T_c$ the table shows measured data with errors due to the 6% systematic error. Both values and errors for $T \le T_c$ are obtained by the fit in the low energy limit $W \to 0$, taking into account the error matrix. The last value at $T = 0.14$ K was out of the RAP experimental reach, and is derived by extrapolating the fit of Eq. (9) also with respect to temperature. The right column shows the predictions of the model (see Section 2).

Temperature (K)	Experimental B/W $(10^{-10}\,mJ^{-1})$	Predicted B/W $(10^{-10}\,mJ^{-1})$
264	2.14 ± 0.13	2.23
71	2.18 ± 0.13	2.23
4.5	2.09 ± 0.13	1.80
1.5	2.25 ± 0.13	1.72
0.8	-0.95 ± 2.4	−7.3
0.7	-4.2 ± 2.5	−7.9
0.6	-6.9 ± 2.5	−7.7
0.35	-10.8 ± 2.3	−9.1
0.14	-11.1 ± 1.8	n/a

Using this table we can estimate:

$$\frac{B/W_{T=0.14\,K}}{B/W_{T=1.5\,K}} = 4.9 \pm 0.8 \quad (12)$$

in good agreement with the value 4.3 ± 1.5 obtained comparing cosmic rays detected in NAUTILUS at $T = 0.14$ K and $T = 3$ K. We assume in the next section that this value does not change in the range 1.5–4.5 K.

5. Cosmic Rays in *gw* acoustic detectors—interpretation in the light of RAP results

The aim of this paper is to use the RAP results to interpret the cosmic ray signals detected in the EXPLORER and NAUTILUS *gw* antennas. To this purpose, we first summarize the most relevant results on this issue [33,34].

The ultra-cryogenic acoustic *gw* detector NAUTILUS [2,35] is operating since 1996 at the INFN Frascati Laboratory, at about 200 m above sea level: it consists of a 3 m, 2300 kg, Al5056 alloy bar. We consider here the run of 1998, when NAUTILUS was operated at 140 mK. The quantity to be observed in this kind of detector (the "*gw* antenna output") is the vibrational amplitude of its first longitudinal mode of oscillation. This is converted by means of an electromechanical resonant transducer into an electrical signal which is amplified by a dc-SQUID superconducting amplifier. The bar and the resonant transducer form a coupled oscillator system, with two resonant modes, whose frequencies were, in that run, $f_- = 906.40$ Hz and $f_+ = 921.95$ Hz. NAUTILUS is equipped with a cosmic ray detection telescope made of seven layers of gas detectors (streamer tubes) for a total of 116 counters [3].

The *gw* detector EXPLORER [36,37], similar to NAUTILUS, was located in CERN (Geneva-CH) at about 430 meters above the sea level. Scintillator counters were installed at EXPLORER in 2002, using scrap equipment recovered after the LEP shutdown. The two detectors have a long record of coincidence runs [38], also with other detectors [39], to search for *gw* signals.

The signal expected in a *gw* detector like NAUTILUS, as a consequence of the interaction of a particle releasing an energy W (Refs. [4,40,41]), according to the model described in Section 2, is (W in GeV units):

$$E \sim \frac{7.64}{2} \times 10^{-9} W^2 \delta^2 \quad \text{[K]} \tag{13}$$

where the bar oscillation energy E is expressed, as usual in the antenna jargon, in Kelvin units ($1\ \text{K} = 1.38 \times 10^{-23}$ J), the numerical constant is the value computed using the thermal expansion coefficient and the specific heat of pure aluminum at 4 K and δ is a parameter that describes the difference respect to pure aluminum at 4 K. In the previous section we have shown that RAP has measured $\delta_n = 1.16$ above the s transition temperature or $\delta_s = 5.7 (= 4.9 \times 1.16)$ for superconductive Al5056. The vibrational energy E of the first longitudinal mode of oscillation is proportional to the square of the Amplitude (in an oversimplified model, $E = \frac{1}{4} M \omega_0^2 B^2$). The constant 7.64×10^{-9} applies if the energy is released in the bar center. If the energy is uniformly distributed along the bar, as in the case of extensive air showers (EAS), this value is reduced by a factor 2.

Under simplified approximations on the development of the electromagnetic shower in the bar, we can derive [4,40,41] the relation between the vibrational energy detected in the bar and the density Λ of secondaries in the shower:

$$E = 4.7 \times 10^{-10} \Lambda^2 \delta^2 \quad \text{[K]}. \tag{14}$$

The plot of vibrational energy E_{exp} *vs* particle density Λ is shown in Fig. 10. In this figure we show the events detected by NAUTILUS, both at 140 mK and at 2.6 K, as well as by EXPLORER at a temperature of about 3 K. We clearly see a difference of more than one order of magnitude between the measurements taken with aluminum in the s state and those in n conduction state. From this plot we can estimate a value of $\delta_s = 5.0 \pm 1.8$ in good agreement with the value derived by the RAP experiment: $\delta_s = 5.7 \pm 0.9$.

We now briefly discuss the event rate of cosmic rays in *gw* detectors. The cosmic ray event rate in NAUTILUS and EXPLORER has been evaluated in the past considering three different event categories: (i) pure electromagnetic showers, responsible for most of the high energy events detected in the bar detectors; (ii) showers produced by muons; and (iii) showers produced by hadrons in the bar. We use Eq. (13) with the correction $\delta_n = 1.16$ for the response of an Al5056 bar in the n state. The rate of electromagnetic air showers (EAS) is computed starting from the empirical relation due to Cocconi [42]. The event rate due to muon and hadron interactions inside the bar was computed using the GEANT package [43], to simulate the antenna and the CORSIKA Monte Carlo [44], as input to GEANT, to simulate the effect of the hadrons produced by the cosmic ray interactions in the atmosphere, assuming a cosmic ray "light" composition. The Monte Carlo simulation represents 1 year of data taking.

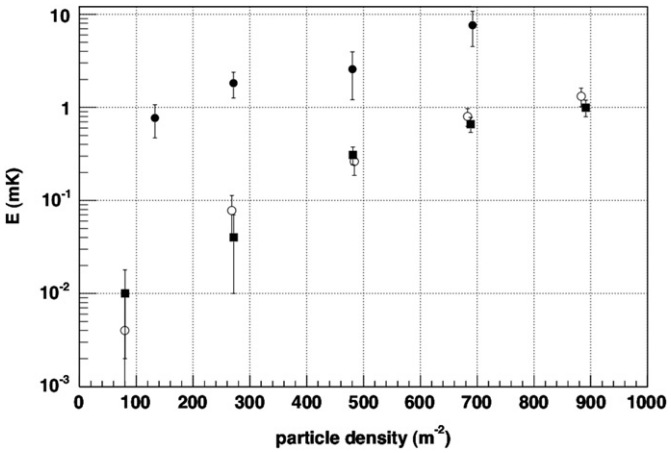

Fig. 10. Averages of signals with energy $E_{exp} \leq 0.1$ K, grouping data in ranges of particle density Λ. Filled circles: NAUTILUS at $T = 0.14$ K, open circles: NAUTILUS at $T = 3$ K, filled squares: EXPLORER at $T = 3$ K. The data gathered at $T = 0.14$ K are roughly one order of magnitude larger than those collected at $T = 3$ K. From Ref. [34].

Table 4
Estimated rate of antenna excitations due to cosmic rays in NAUTILUS *vs* the vibrational energy of the longitudinal fundamental mode that such events can produce. The value at $E = 0.1$ K is obtained extrapolating from the lower energy values. The values in the second column are the values of cosmic ray energy that the bar needs to absorb in order to have an excitation energy E. Vibrational and deposited energy are correlated by Eq. (13), under the assumption of uniformly distributed energy.

Vibrational E (K)	Deposited W (GeV)	Total (events/day)
$\geq 10^{-5}$	≥ 44.5	107
$\geq 10^{-4}$	≥ 141	14.5
$\geq 10^{-3}$	≥ 445	1.6
$\geq 10^{-2}$	≥ 1410	0.19
$\geq 10^{-1}$	≥ 4450	0.03

The results are shown in Table 4. The energy in the first longitudinal mode E (first column) is proportional to the square of the absorbed energy W.

The rate of the events scales as $W^{-0.9}$. This is because the cosmic ray integral spectrum is well described by a power law $E_{CR}^{-\beta}$ with $\beta \sim 1.7$ for cosmic ray primaries up to the so called "knee" at $E_{CR} = 10^{15}$ eV and $\beta \sim 2$ at higher energies.

In Ref. [40], very large NAUTILUS signals at a rate much greater than expected, when the antenna was operated at $T = 140$ mK, were reported. In the light of the analysis reported above, it is now clear that the value $\delta_s = 5.7$ must be used in Eq. (14) to compute the expected response and the expected rate. The NAUTILUS 1998 data event rate per day after the unfolding of the background, with the procedure described in Ref. [34] is shown in Fig. 11. The continuous line is the prediction of Table 4 with $\delta_s = 5.7$. We find now a good agreement between measurements and predictions; previously hypothesized exotic explanations, based on anomalous component of cosmic rays or anomalous interactions of cosmic rays with a superconductive bar can now be excluded.

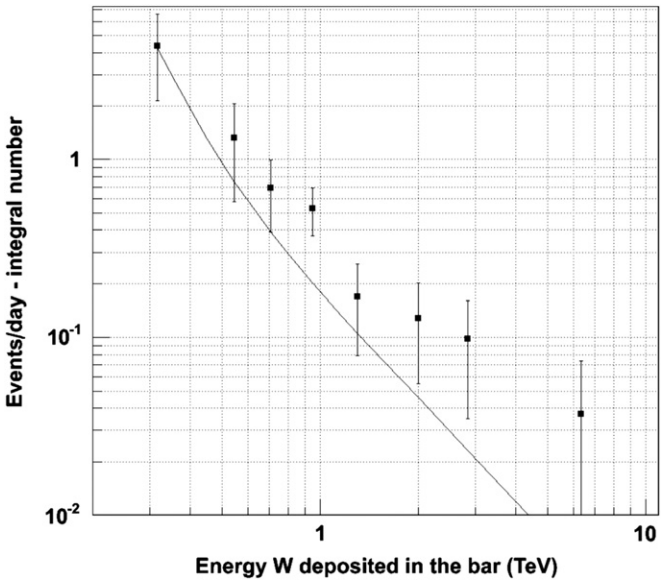

Fig. 11. NAUTILUS 1998 data, at $T=0.14$ K. The integral distribution of the event rate after the background unfolding, compared with the expected distribution (continuous line). The prediction is computed using the data of Table 4 and using the value $\delta_s = 5.7$ measured by RAP. The good agreement suggests the absence of anomalous components of cosmic rays or anomalous interactions of cosmic rays with a superconductive bar. Modified from Ref. [34].

With this analysis cosmic ray showers have been turned from a nuisance to a very important tool to verify the sensitivity of *gw* bar detectors to signals distributed along the bar, signals similar to *gw* even if the excitation mechanism is different. Moreover the cumulative analysis of Fig. 10 and the agreement with the RAP measurements show that for this kind of search the sensitivity of bar detectors can be studied down to 10 μK corresponding to $B < 10^{-19}$ m. This results is quite important for other "cumulative" analysis like the search of signals from gamma ray bursts.

Finally, we remark that acoustic *gw* detectors have no limitations due to saturation effects in detecting large signals. Indeed the largest event detected up to now has a vibrational energy in the first longitudinal mode $E \sim 670$ K corresponding to ~ 360 TeV in the bar. The event occurred in EXPLORER on Nov 10 2006 9:40 UT.

6. Conclusions

We have shown that the Thermo-Acoustic Model describes reasonably well the response of a bar to the passage of ionizing particles. At high temperatures, in a normal conduction state, the prediction, based on the knowledge of the Grüneisen parameter, is in a good agreement with the data. In a superconductive material, the transitions between the s and n state complicate this picture. Due to the poor knowledge of the low temperatures parameter and to the approximations of the model, a direct measurement with a particle beam was needed to directly measure the response to ionizing particles. The RAP experiment addressed this issue. At high energy densities of the impinging particles, we have detected and studied with RAP nonlinear effects that complicate the data analysis.

We have shown that the unexpected large events detected in 1998 with NAUTILUS at $T=0.14$ K were due to its superconductive state. Using the RAP measurements we have regauged the rate of cosmic rays detected by the NAUTILUS and EXPLORER antennas, and shown that they are in agreement with the predictions.

Currently the background due to cosmic rays in acoustic bar detectors is negligible. This is because the typical sensitivity is $E=1$ mK; the standard event selection requires a threshold of about 25 mK. With such a threshold we have a few events per week due to cosmic rays. These events are, however, very useful as a tool to continuously monitor and calibrate the acoustic *gw* detectors. Moreover, in the standard NAUTILUS data analysis, these events are currently vetoed and removed by the official *gw* event list.

Cosmic rays will represent an important source of background in future higher sensitivity [7], possibly superconducting, detectors, and this noise should be taken into account in acoustic [45–47] detectors. To remove this background, moving to an underground site could be necessary.

Acknowledgement

We gladly acknowledge precious help from our technicians M. Iannarelli, E. Turri, F. Campolungo, R. Lenci and F. Tabacchioni. This work was partially funded by the EU Project ILIAS (RII3-CT-2004-506222).

References

[1] D.H. Ezrow, N.S. Wall, J. Weber, G.B. Yodh, Phys. Rev. Lett. 24 (1970) 945.
[2] P. Astone, et al., Astropart. Phys. 7 (1997) 231.
[3] E. Coccia, et al., Nucl. Instr. and Meth. A 355 (1995) 624.
[4] P. Astone, et al., Phys. Rev. Lett. 84 (2000) 14.
[5] B. Buonomo, et al., Astropart. Phys. 24 (2005) 65.
[6] P. Astone, et al., Phys. Rev. D 47 (1993) 4770.
[7] K. Yamamoto, et al., Phys. Rev. D 78 (2008) 022004 arXiv:0805.2387 [gr-qc].
[8] A.I. Kalinichenko, G.F. Popov, Radiat. Phys. Chem. 63 (2002) 755.
[9] B.L. Beron, R. Hofstadter, Phys. Rev. Lett. 23 (1969) 184.
[10] B.L. Beron, S.P. Boughn, W.O. Hamilton, R. Hofstadter, T.W. Tartin, IEEE Trans. Nucl. Sci. NS-17 (1970) 65.
[11] A.M. Grassi Strini, G. Strini, G. Tagliaferri, J. Appl. Phys. 51 (1980) 849.
[12] A.M. Allega, N. Cabibbo, Lett. Nuovo Cim. 38 (1983) 263.
[13] C. Bernard, A. De Rujula, B. Lautrup, Nucl. Phys. B 242 (1984) 93.
[14] G. Liu, B. Barish, Phys. Rev. Lett. 61 (1988) 271.
[15] K.S. Wood, D. Van Vechten, Nucl. Instr. and Meth. A 314 (1991) 86.
[16] K.E. Gray, in: A. Barone (Ed.), Proceedings of the Superconductive Particle Detectors, 26–29 October 1987, World Scientific, Singapore, 1988.
[17] N.K. Sherman, Phys. Rev. Lett. 8 (1962) 458.
[18] B. Strehl, et al., Phys. Lett. B 242 (1990) 256.
[19] R.R. Hake, Phys. Rev. 166 (1968) 471.
[20] D. White, et al., Phys. Rev. 109 (1958) 797.
[21] F.R. Kroeger, C.A. Swenson, J. Appl. Phys. 48 (1977) 853.
[22] J.G. Collins, G.K. White, C.A. Swenson, J. Low Temp. Phys. 10 (1972) 69.
[23] CRC Handbook of Chemistry and Physics, 73rd ed., CRC Press, 1992.
[24] M. Barucci, et al., Physica B 405 (2010) 1452.
[25] E. Coccia, T.O. Niinikoski, J. Phys. E: Sci. Instr. 16 (1983) 695.
[26] E.F. Harris, D.E. Mapother, Phys. Rev. 165 (1968) 522.
[27] E. Coccia, T.O. Niinikoski, Lett. Nuovo Cim. 41 (1984) 242.
[28] S. Boughn, et al., Rev. Sci. Instr. 61 (1990) 1.
[29] B. Buonomo, G. Mazzitelli, F. Murtas, L. Quintieri, in: Proceedings of EPAC-2008, June 23–27, 2008, Genoa, Italy.
[30] B. Buonomo, G. Mazzitelli, F. Murtas, L. Quintieri, P. Valente, in: Proceedings of Beam Instrumentation Workshop May 4–8, 2008, Lake Tahoe, California, USA.
[31] M. Barucci, et al., Phys. Lett. A 373 (2009) 1801 arXiv:0901.1220 [gr-qc].
[32] M. Bassan, et al., Europhys. Lett. 76 (2006) 987.
[33] F. Ronga, et al., ROG and RAP Collaborations, Nucl. Phys. B Proc. Suppl. 190 (2009) 44.
[34] P. Astone, et al., Astropart. Phys. 30 (2008) 200 arXiv:0806.1335 [hep-ex].
[35] P. Astone, et al., Europhys. Lett. 16 (1991) 231.
[36] E. Amaldi, et al., Nuovo Cim. C 7 (1984) 338.
[37] P. Astone, et al., Phys. Rev. D 47 (1993) 362.
[38] P. Astone, et al., Class. Quant. Grav. 18 (2001) 243.
[39] P. Astone, et al., Phys. Rev. D 82 (2010) 022003 and references therein.
[40] P. Astone, et al., Phys. Lett. B 499 (2001) 16.
[41] P. Astone, et al., Phys. Lett. B 540 (2002) 179.
[42] G. Cocconi, in: S. Flugge (Ed.), Encyclopedia of Physics, vol. 46(1), 1961, p. 228.
[43] ⟨http://wwwasd.web.cern.ch/wwwasd/geant/⟩.
[44] D. Heck, et al., Report FZKA 6019, Forschungszentrum Karlsruhe, 1998.
[45] M. Bonaldi, et al., Phys. Rev. D 74 (2006) 022003 arXiv:0605004 [gr-qc].
[46] L. Gottardi, et al., Phys. Rev. D 76 (2007) 102005.
[47] E. Coccia, et al., Phys. Rev. D 57 (1998) 2051.